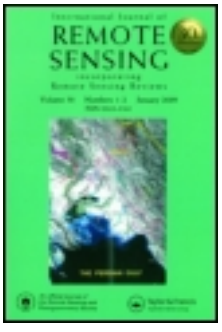

International Journal of Remote Sensing

Publication details, including instructions for authors and subscription information:
http://www.tandfonline.com/loi/tres20

Improving flood monitoring by the Robust AVHRR Technique (RAT) approach: the case of the April 2000 Hungary flood

T. Lacava [a], C. Filizzola [a], N. Pergola [a b], F. Sannazzaro [a] & V. Tramutoli [b a]

[a] Institute of Methodologies for Environment Analysis (IMAA), National Research Council (CNR), c. da Santa Loja, 85050, Tito Scalo (PZ), Italy

[b] Department of Engineering and Physics of Environment (DIFA), University of Basilicata, via dell'Ateneo Lucano 10, 85100, Potenza, Italy

Available online: 28 Apr 2010

To cite this article: T. Lacava, C. Filizzola, N. Pergola, F. Sannazzaro & V. Tramutoli (2010): Improving flood monitoring by the Robust AVHRR Technique (RAT) approach: the case of the April 2000 Hungary flood, International Journal of Remote Sensing, 31:8, 2043-2062

To link to this article: http://dx.doi.org/10.1080/01431160902942902

International Journal of Remote Sensing
Vol. 31, No. 8, 20 April 2010, 2043–2062

Taylor & Francis
Taylor & Francis Group

Improving flood monitoring by the Robust AVHRR Technique (RAT) approach: the case of the April 2000 Hungary flood

T. LACAVA*†, C. FILIZZOLA†, N. PERGOLA†‡, F. SANNAZZARO† and V. TRAMUTOLI‡†

†Institute of Methodologies for Environment Analysis (IMAA), National Research Council (CNR), c. da Santa Loja, 85050 Tito Scalo (PZ), Italy

‡Department of Engineering and Physics of Environment (DIFA), University of Basilicata, via dell'Ateneo Lucano 10, 85100 Potenza, Italy

(*Received 11 January 2008; in final form 12 June 2008*)

In the past, satellite remote sensing techniques have been widely used within the flood risk management cycle. In particular, there have been many demonstrations of the operational use of satellite data for detailed monitoring and mapping of floods and for post-flood damage assessment. When frequent situation reports are requested (e.g. in the emergency phase or for early warning purposes) to assist civil protection activities, high temporal resolution satellites (mainly meteorological, with revisiting times from hours to minutes) can play a strategic role. In this paper, a new Advanced Very High Resolution Radiometer (AVHRR) technique for monitoring flooded areas is presented. Its performances are evaluated in comparison with other well-known approaches, analysing the flood event that occurred in Hungary during April 2000 involving the Tisza and Timis Rivers. The preliminary results seem to indicate the benefits of such a new technique, especially when different observational conditions are considered. In fact, compared with previously proposed techniques, the proposed approach: (a) is completely automatic (i.e. unsupervised with no need for operator intervention); (b) improves flooded-area detection capabilities strongly reducing false alarms; and (c) automatically discriminates (without the need for ancillary information) flooded areas from permanent water bodies. Moreover, it is globally applicable and, because of the complete independence on the specific satellite platform, is easily exportable to different satellite packages.

1. Introduction

Remote sensing data have been widely used within the hydro-meteorological risk management cycle: satellite data have been shown to be an excellent tool for providing hydrological information including the quantification of physical characteristics of catchments, such as topography and land use, and meteo-dependent parameters, such as soil moisture and snow cover. Moreover, there have been many demonstrations of the operational use of satellites for detailed monitoring and mapping of floods and post-flood damage assessment (CEOS 2001, 2003 and references therein).

Mapping and monitoring of flooded areas are fundamental, during both the emergency and the recovery (post-emergency) phases. Timely and frequently updated

*Corresponding author. Email: lacava@imaa.cnr.it

International Journal of Remote Sensing
ISSN 0143-1161 print/ISSN 1366-5901 online
http://www.tandf.co.uk/journals
DOI: 10.1080/01431160902942902

situation reports are particularly required, by the local authorities, during the emergency phase in order to locate and identify the affected areas and to consequently organize rescue and damage-mitigation actions. Optical instruments aboard polar and geostationary meteorological satellites can offer, despite their low spatial resolution (from a few kilometres up to a few hundreds of metres), temporal resolutions (from a few hours up to a few tens of minutes) that are high enough to guarantee timely, frequent and updated situation reports, in the absence of clouds. In addition, the availability of several satellite passes per day gives more chances to achieve cloud-free images (Sandholt *et al.* 2003, Jain *et al.* 2006).

More detailed information (i.e. at higher spatial and/or spectral resolution) is required, even after the emergency, for a first assessment of damage and for updating risk maps (McGinnis and Rango 1975, Pultz *et. al.* 1991). Different satellite packages exist that offer excellent flood-mapping capabilities, with even longer (from weeks to tens of days) revisiting time. Detailed ground information, at spatial resolutions from tens of metres to tens of centimetres, can be achieved by medium- to high-spatial-resolution optical satellite sensors (on board Landsat, Defence Meteorological Satellite Program (DMSP), Systeme Pour l'Observation de la Terre (SPOT), Indian Remote Sensing (IRS), Ikonos, QuickBird, etc.; CEOS 2003) in absence of clouds. Active microwave satellite sensors (such as the Synthetic Aperture Radar (SAR) on board European Remote Sensing (ERS), Environmental Satellite (ENVISAT), Radar Satellite (RADARSAT), etc.) can also assure effective (with spatial resolutions of tens of metres) and reliable maps of flooded areas also in the presence of (not raining) clouds, but, up to now, with the same revisiting time limits of high-spatial-resolution sensors.

Owing to its short revisiting time (less than 6 hours) and low image-acquisition cost, despite its relatively moderate spatial resolution (1.1 km at nadir), National Oceanic and Atmospheric Administration/Advanced Very High Resolution Radiometer (NOAA/AVHRR) data have been used for a long time for real-time flooding-disaster monitoring.

Several techniques have been proposed (e.g. Winsnet *et al.* 1974, McGinnis and Rango 1975, Cao *et al.* 1987, Xiao and Chen 1987, Ali 1989, Barton and Bathols 1989, Lin 1989, Verdin 1996, Sheng and Xiao 1998, Islam and Kimitera 2000, Sheng and Gong 2001, Jain *et al.* 2006) that exploit the different spectral response of the water and soil in the visible (channel 1, 0.58–0.68 μm), near infrared (channel 2, 0.725–1.00 μm) and thermal infrared (channel 4, 10.30–11.30 μm and channel 5, 11.50–12.50 μm) AVHRR bands, to detect and map flooded areas. In fact, compared with other land-surface covers (see figure 1), water shows:

- a lower reflectance in AVHRR channel 2 (R_2) so that, in the presence of water bodies, lower values of R_2 are expected;
- a relatively higher reflectance in AVHRR channel 1 (R_1) than in channel 2 (R_2) so that, in the presence of water bodies, lower values of R_2 / R_1 and $R_2 - R_1$ are expected; and
- a lower daily thermal range so that, in the presence of water bodies, a higher signal in thermal AVHRR channel 4 (T_4) during the night (lower during the day) is expected.

Other AVHRR-based products, such as the Normalized Difference Vegetation Index (NDVI), (e.g. McFeeters 1996, Hasegawa *et al*. 1998, Domenikiotis *et al.* 2003, Wang *et al.* 2003, Jain *et al.* 2005, Liu *et al.* 2005 and references therein) and Surface Temperature (ST) (e.g. Domenikiotis *et al.* 2003) have also been proposed in order to provide information that is useful for flooding-damage assessment purposes.

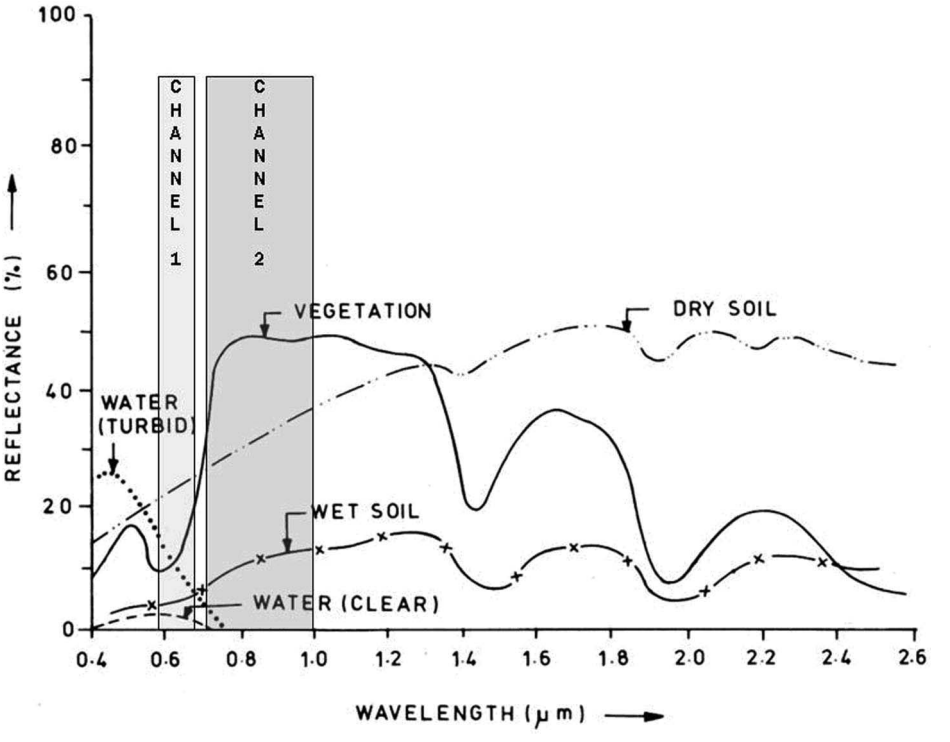

Figure 1. Typical reflectance (%) signatures obtained in laboratory for soil, water and vegetation (adapted from Gupta (1991), reprinted with kind permission of Springer Science + Business Media).

Even if potentially useful in order to delimitate flooded areas, such products can work only after the time and localization of a flooding event have been independently provided (Domenikiotis *et al.* 2003, Wang *et al.* 2003), so they are not useful for early warning purposes.

2. Previous main AVHRR satellite techniques for flooded-area monitoring

Main AVHRR satellite techniques for flooded-area monitoring are simply devoted to discriminating water bodies from soils. This is generally done by applying, to every image pixel, the same very simple, fixed-threshold test that, on the basis of measured AVHRR radiances, permits us to establish if the corresponding ground resolution cell is water affected or not. This means that a suitable land/water discrimination threshold value S_0 is chosen and applied all over the scene. A selection of classical AVHRR-based fixed-threshold tests used to discriminate water bodies from soils can be found in table 1. In order to choose an appropriate S_0 threshold, all these methods are based on the interactive analysis of the histograms obtained from R_2 (Lin 1989), R_2 / R_1 (Sheng and Xiao 1998), $R_2 - R_1$ (Xiao and Chen 1987) or T_4 (Barton and Bathols 1989, Verdin 1996) AVHRR images, where land and water pixels usually appear arranged in a bi-modal distribution. The S_0 threshold is then interactively chosen in the region between the two peaks corresponding to the maximum frequency of land and water pixels (e.g. Sheng and Xiao 1998). All these techniques, using S_0 thresholds

Table 1. Classic AVHRR based fixed threshold tests (see text) for discriminating water bodies from soil.

Authors reference	Applied test: water if	Daytime (D) or Nighttime (N) tests
Xiao and Chen (1987)	$R_2 - R_1 \leq S_0$	D
Barton and Barthols (1989)	$T_4 \geq S_0$	N
Lin (1989)	$R_2 \leq S_0$	D
Verdin (1996)	$T_4 \leq S_0$	D
Sheng and Xiao (1998)	$R_2 / R_1 \leq S_0$	D

chosen in place (i.e. just on the basis of the satellite image at hand), share the advantage of being exportable to different satellite packages and geographic areas, showing fairly good performances, even under very different observational conditions. Among the others, the Sheng and Xiao (1998) method based on the ratio R_2 / R_1 seems to be (according to Sheng and Gong (2001)) more protected against spurious effects (due, for instance, to the presence of cloud shadows) and able to operate satisfactorily, even in more critical conditions (e.g. in the presence of thin clouds). Some limitations still exist that affect (in different ways) all the above-mentioned techniques and are mainly related to the following issues.

- *Not univocal S_0 threshold choice*. The S_0 threshold is sometimes difficult to identify because of the absence of a clear bi-modal distribution in the image histogram. This might depend on different factors related to a relatively poor abundance of water-body (with respect to land) pixels in the scene or a low (or even inverted) land/water contrast, in comparison with its expected behaviour, in particular observational conditions. This is the case, for instance, of observations made close to dawn or dusk time (for tests based on T_4) or in the presence of 'dark bodies', such as lateritic upland areas (Verdin (1996) and references therein) or cloud shadows (Sheng and Xiao 1998), which particularly affect tests using R_2 images. A possible contribution from spurious sources, such as residual clouds (not perfectly identified and excluded in the pre-processing steps), cloud shadows, snow and, particularly close to the coasts, sun-glint effects that, by erroneously populating the water part of the histogram, can destroy its bi-modal distribution, generate additional peaks, or just shift the positions of peak maxima.
- *Expert supervision required.* As a direct consequence of the above-mentioned problems, the determination of S_0 requires the assistance of an operator. In addition to introducing subjective interpretation elements, this is an unfavourable circumstance for a real-time monitoring activity. These subjective elements also affect the preliminary decision on the extension of the area to be selected in order to apply the histogram-based S_0 determination process. In fact, performances of fixed-threshold methods usually improve when they are selectively applied to flooded areas of limited extension and in the absence of clouds. This makes them more effective in the disaster-assessment phases or, more generally, when the area to be investigated has been independently and preliminarily identified and restricted.
- *False identification.* Even in the case that the S_0 threshold can suitably be chosen by the histogram method, false identification of flooded areas may occur that is related to local observational conditions (e.g. snow, cloud shadow, etc.).

- *Complicated discrimination between permanent water bodies and newly flooded areas.* All the above-mentioned fixed-threshold methods are firstly devoted to discriminate water from land pixels, so that further processing steps are required in order to discriminate flooded areas from natural water bodies (e.g. normal river or lake shapes) present in the investigated area. Usually, this is done by comparing the water/land mask with a similar satellite (as in Verdin (1996), Sheng and Gong (2001)) or ground-based products describing water-body distribution in normal conditions (i.e. no floods in action). This is generally not a difficult task but the estimated amount of flooded areas will depend, not only on the reliability of the used water detection method, but also on the quality of the available pre-flood water-bodies map.

In this paper, a new AVHRR technique for real-time monitoring of flooded areas, which seems able to overcome the above-mentioned limitations, is presented. It is based on the general Robust AVHRR Technique (RAT), recently changed to the Robust Satellite Techniques (RST) approach (Tramutoli 1998, 2005) already successfully applied to forest-fire detection (Cuomo *et al.* 2001), volcanic eruption (Pergola *et al.* 2001, 2004, Di Bello *et al.* 2004) seismic-area monitoring (Tramutoli *et al.* 2001, 2005, Filizzola *et al.* 2004, Corrado *et al.* 2005), cloud detection (Cuomo *et al.* 2004) and hydrologic risk evaluation (Lacava *et al.* 2005a,b,c, 2006). In this work, the RAT approach is applied to the real-time mapping of flooded areas for the first time. Its implementation will be described and results discussed (also for comparison with some of the previously mentioned techniques) in the case of the flood event that affected eastern Europe from 5 to 21 April 2000, hitting, in particular, the Carpathian Basin and the oriental portion of the Danube Basin (figure 2). The event caused about ten fatalities, the evacuation of 20 000 people and damage to the infrastructures and farmlands (France Press Agency 2000). The country that was mainly affected by the flood was Hungary, with the Danube tributaries (in particular Tisza and Timis Rivers) playing a major role (Brakenridge *et al.* 2003).

3. Proposed methodology

The RAT approach identifies signal anomalies in the space–time domain as deviations from a normal signal behaviour that has previously been determined, at the image pixel level, on the basis of satellite observations collected during several years in the past, under similar observational conditions. A detailed description of the theoretical background of the RAT approach can be found in Tramutoli (1998) as well as in several papers describing its applications (Tramutoli *et al.* 2001, Pergola *et al.* 2004, Lacava *et al.* 2005c, Tramutoli 2005).

Briefly, the RAT approach is an automatic change-detection scheme that considers a satellite image as a space–time process, described at each place (x,y) and time t, by the value of the satellite-derived measurement $V(x,y,t)$. In order to identify anomalous signal transients, an Absolutely Local Index of Change of Environment (ALICE) is then computed as follows:

$$\otimes_{\mathrm{v}}(x,y,t) = \frac{V(x,y,t) - V_{\mathrm{ref}}(x,y)}{\sigma_{\mathrm{v}}(x,y)}, \tag{1}$$

where the signal $V(x,y,t)$ is the measurement achieved at the place (x,y) and time t in a single spectral channel or in a combination of different spectral bands, $V_{\mathrm{ref}}(x,y)$ and

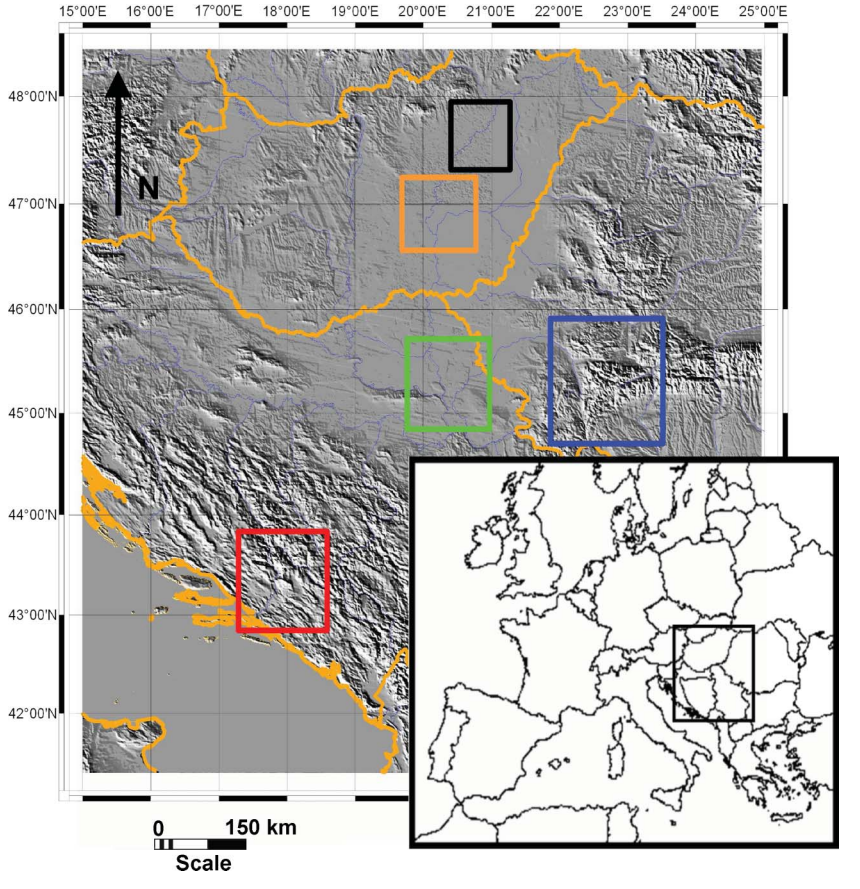

Figure 2. Localization of the investigated area. In the background the Digital Elevation Model (DEM) courtesy of the U.S. Geological Survey (http://eros.usgs.gov/#/Find_Data/Products_and_Data_Available/gtopo30_info). Rivers have been coloured in light blue, while mainly political boundaries are in orange. Differently coloured boxes indicate (flooded and not flooded) test areas quoted in the text.

$\sigma_v(x,y)$ are reference fields (images) describing, for each location (x,y), the expected signal, and its corresponding variability, in unperturbed conditions. Reference fields $V_{ref}(x,y)$ and $\sigma_v(x,y)$ are computed (e.g. as the time average and standard deviation) from historical records collected by the same satellite sensor, under observational conditions as similar as possible (e.g. same period of the year, same time of satellite pass, etc.) to those of the image to be processed. The robustness of this approach is intrinsic because the higher the variability $\sigma_v(x,y)$ of the signal is, the harder it will be to achieve high values of $\otimes_v(x,y)$, reducing, in this way, the problem of false alarms. Owing to this preliminary characterization of the expected signal behaviour, which is specific for the time and the site of observation, the RAT approach allows us to overcome the difficulties (e.g. site effects) arising when a unique threshold is applied in very different observational contexts.

In this work, the RAT approach was applied for real-time flooded-area monitoring by using the same spectral signatures used by Xiao and Chen (1987) and Sheng and Xiao (1998) to build two ALICE indexes:

$$\otimes_{2-1}(x,y,t) = \frac{R_{2-1}(x,y,t) - \mu_{2-1}(x,y)}{\sigma_{2-1}(x,y)} \tag{2}$$

and

$$\otimes_{2/1}(x,y,t) = \frac{R_{2/1}(x,y,t) - \mu_{2/1}(x,y)}{\sigma_{2/1}(x,y)}, \tag{3}$$

where $R_{2-1}(x,y,t) = R_2(x,y,t) - R_1(x,y,t)$ is the difference, and $R_{2/1}(x,y,t) = R_2(x,y,t) / R_1(x,y,t)$ the ratio, between R_2 and R_1 AVHRR bands computed pixel-by-pixel on the AVHRR image at hand; $\mu_{2-1}(x,y)$ and $\mu_{2/1}(x,y)$ are the time averages and $\sigma_{2-1}(x,y)$ and $\sigma_{2/1}(x,y)$ the standard deviations of $R_{2-1}(x,y,t)$ and $R_{2/1}(x,y,t)$ time series computed on a selected multi-year dataset of co-located, cloud-free, AVHRR records collected around the same time of day during the same month of the year.

The index $\otimes_{2-1}(x,y,t)$ (or $\otimes_{2/1}(x,y,t)$) gives, for each location (x,y), the present $R_{2-1}(x,y,t)$ (or $R_{2/1}(x,y,t)$), deviation from its expected (in unperturbed conditions) value, $\mu_{2-1}(x,y)$ (or $\mu_{2/1}(x,y)$), for the same place (x,y) and period of observation, weighted by its normal variability $\sigma_{2-1}(x,y)$ (or $\sigma_{2/1}(x,y)$), as historically observed for the same place under similar observational conditions.

In this case, we expect that:

- the lower $\otimes_{2-1}(x,y,t)$ (or $\otimes_{2/1}(x,y,t)$) index values will appear associated with flooded zones;
- unperturbed zones (including natural water bodies, snow covered mountains, vegetated areas, etc.) will appear associated with higher (close to zero or positive) $\otimes_{2-1}(x,y,t)$ (or $\otimes_{2/1}(x,y,t)$) values;
- there will be an overall reduction of false identifications related to site effects; and
- there will be an improved capability to identify actual flooded areas, directly discriminating them not just from land, but also from permanent water bodies.

In fact, as we can likely expect, the same site, observed under similar observed conditions, will exhibit (in the range of normal variability described by $\sigma_{2-1}(x,y)$ and $\sigma_{2/1}(x,y)$), similar surface features and signal behaviour; therefore, permanent water bodies or perennial snow should not give an anomalous signal and, as a consequence, they should not appear within the flooded pixel class. Only newly affected water areas, exhibiting significant signal deviation (because they are outside the range of the normal variability described by $\sigma(x,y)$ for each specific location), will be detected and included in the flooded image pixel class.

4. Implementation

The proposed approach has been applied, in order to assess its actual potential and efficiency, during the flooding event that affected the Carpathian Basin in April 2000.

To apply the proposed approach to this event, firstly a dataset related to diurnal AVHRR passes, collected between 11:00 and 15:00 GMT, was chosen. As mentioned earlier, a single NOAA satellite is able to guarantee at least two passes per day at around the same solar local time. Moreover, the current NOAA satellite constellations allow us a very short revisiting time (less than six hours), so that, in the selected temporal slot, we were able to collect at least one image each day of the chosen month. The dataset consisted of about 110 images acquired in the month of April over 5 years (1995–1999). Subsequently, all the images were processed (calibrated and navigated

with subpixel accuracy by using Subpixel Automatic Navigation for AVHRR (SANA); Pergola and Tramutoli 2000, 2003) and co-located in the space–time domain in the same (Lambert Azimuthal Equal Area) geographic projection. The reference fields ($\mu_{2-1}(x,y)$, $\mu_{2/1}(x,y)$, $\sigma_{2-1}(x,y)$ and $\sigma_{2/1}(x,y)$), representing signal behaviour under unperturbed conditions, were generated, at pixel level, for the region of interest. Figure 3 shows the reference fields corresponding to the signal behaviour expected for the month of April in the time slot 11:00–15:00 GMT as obtained on the basis of 5 years (1995–1999) of AVHRR record analysis. All AVHRR records corresponding to cloudy pixels – identified by applying the One-channel Cloud-detection Approach (OCA) to AVHRR channels 2 and 4 (Pietrapertosa *et al.* 2001, Cuomo *et al.* 2004) – have been excluded during the reference-field computation process. Due to their spectral signature, natural water bodies, as expected, are well delineated by the darkest grey tones (lowest corresponding values) in the $\mu_{2-1}(x,y)$ and $\mu_{2/1}(x,y)$ reference images. Lighter grey tones (highest corresponding values) in the $\sigma_{2-1}(x,y)$ and $\sigma_{2/1}(x,y)$ reference images highlight pixels affected by higher signal variability.

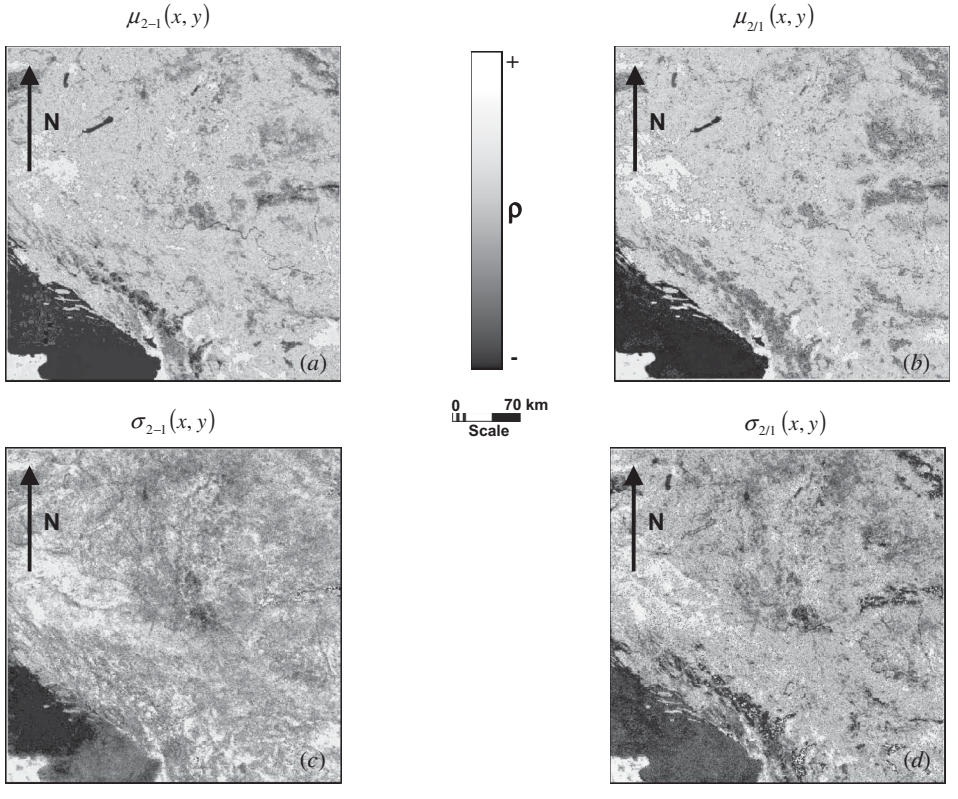

Figure 3. Reference fields computed for the month of April in the time-slot 11:00-15:00 GMT: (*a*) and (*b*) are the mean of the difference and ratio between channel 2 and channel 1 AVHRR respectively, in which bright colours are high values and dark colours are low values of reflectance; (*c*) and (*d*) are standard deviation of the difference and ratio between channel 2 and channel 1 AVHRR respectively, in which bright colours are high values and dark colours are low values of variability.

For all AVHRR images of the considered study case, the ALICE indexes $\otimes_{2\_1}(x,y,t)$ and $\otimes_{2/1}(x,y,t)$ (denoted in the text as $\otimes_{2\_1}$ and $\otimes_{2/1}$ from here onwards) have been computed and results were analysed.

In the following, first achievements obtained by applying the RAT approach to the April 2000 flooding event will be presented and discussed, and will be compared with the results achieved by the application of some of the above-mentioned fixed-threshold approaches.

5. Results

The areas hit by the flood that occurred in the Carpathian Basin in April 2000 have been analysed before, during and after the event. Results achieved by the proposed methodology will be compared (excluding cloudy AVHRR images) with the ones achieved from the application of the other traditional fixed-threshold AVHRR techniques in order to evaluate improvements in flooded-area detection in terms of robustness (against false identifications) and detection capability.

Both $\otimes_{2\_1}$ and $\otimes_{2/1}$ ALICE indexes have been considered that, as previously stated, are based on the same $R_{2\_1}(x,y,t) = R_2(x,y,t) - R_1(x,y,t)$ and $R_{2/1}(x,y,t) = R_2(x,y,t) / R_1(x,y,t)$, AVHRR spectral signatures used by Xiao and Chen (1987) and Sheng and Xiao (1998).

AVHRR pixels exhibiting $\otimes_{2\_1} \leq -1$ (i.e. having $R_{2\_1}(x,y,t) \leq \mu_{2\_1}(x,y) - \sigma_{2\_1}(x,y)$) or $\otimes_{2/1} \leq -1$ (i.e. having $R_{2/1}(x,y,t) \leq \mu_{2/1}(x,y) - \sigma_{2/1}(x,y)$) have preliminarily been considered as flooded by considering their spectral signatures affected by the presence of water for an amount greater than the normal variability of the considered signal, as historically observed at the same place and in the same period of the year.

First of all, we have verified the reliability of our approach in the identification of flooded area: a test has been performed by comparison with a SAR image collected over a portion of the area (within the green box of figure 2) affected by the studied flooding event on 13 April 2000 (figure 4). As is well known (even if with a temporal resolution which is much lower than the one offered by AVHRR systems), such active microwave satellite systems are able to offer (even in the presence of cloud coverage) reliable and detailed water/land discrimination products that are particularly useful for damage assessment or, as in our case, for validating other products of satellite observations (e.g. Pultz and Crevier 1996, Saper *et al.* 1996, Pultz *et al.* 1997). The same image has been adapted to highlight the darker areas that should represent water bodies, including flood affected zones used as the background in figure 5 (the main flooded areas are within the circles). In these images, the results of the Xiao and Chen (1987) technique are shown after its application to the AVHRR image (the closest in time to the SAR one and free from clouds over the area) collected around 13:00 GMT on 14 April 2000. Compared with SAR indications, it seems quite evident that such a technique is capable of correctly identifying water-affected pixels. However, such results are not completely satisfactory, since many flooded areas (quite evident on the SAR image) are not identified. The application of the Sheng and Xiao (1998) and Verdin (1989) techniques was not possible for the same day because of the difficulty of univocally identifying S_0 thresholds in the corresponding R_2 / R_1 and T_4 image histograms.

In figures 6(*a*) and 6(*b*), the results obtained by applying $\otimes_{2\_1}$ and $\otimes_{2/1}$ ALICE indexes to the same AVHRR image are shown. In comparison with results achieved

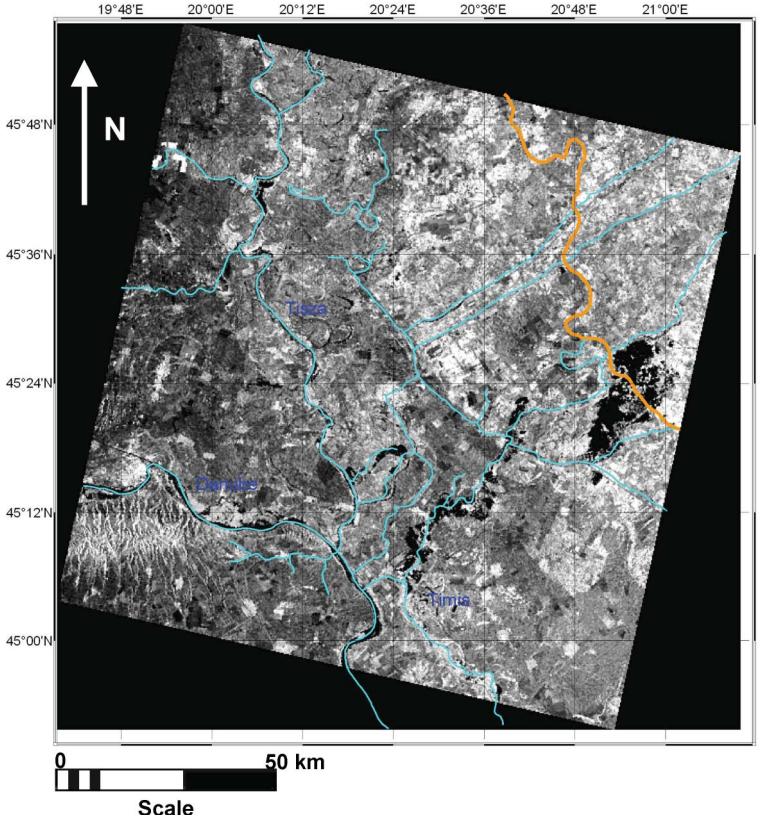

Figure 4. SAR (Synthetic Aperture Radar) image collected from ERS (European Remote Sensing) satellite on 13 April 2000 at 14:00 GMT on the area flood affected corresponding to the green box in figure 2. The rivers have been coloured in cyan while the political boundary between Serbia and Romania is in orange. Adapted from ESA (European Space Agency) product available online at http://earth.esa.int/ew/floods/tisza_hu_00/_images/fl_hu_fu.jpg.

by applying the Xiao and Chen (1987) technique (figure 5), the major detection capabilities offered by the RAT approach are quite evident. In particular, looking at figure 6(*a*), it is possible to note an increase of flooded areas correctly identified by applying the $\otimes_{2-1}$ index: most of the darker flooded pixels identifiable in the SAR image collected on 13 April are identified as flooded. Results achieved by applying the $\otimes_{2/1}$ index (figure 6(*b*)) are quite similar to the ones achieved by the Xiao and Chen (1987) technique. It should be noted, however, that such results are achieved, in the first case, by an unsupervised (i.e. automatic and operationally faster) approach. The comparison between the two proposed indexes seems to indicate that $\otimes_{2-1}$ is more sensitive to the identification of flooded areas, while $\otimes_{2/1}$ is less affected by spurious effects due to isolated signal anomalies that are possibly related to the intrinsic uncertainty in image-to-image co-location and/or to occasional image-navigation errors.

Once the reliability of the proposed index has been verified, we tested if such an approach could overcome the main limits of the traditional AVHRR techniques. At

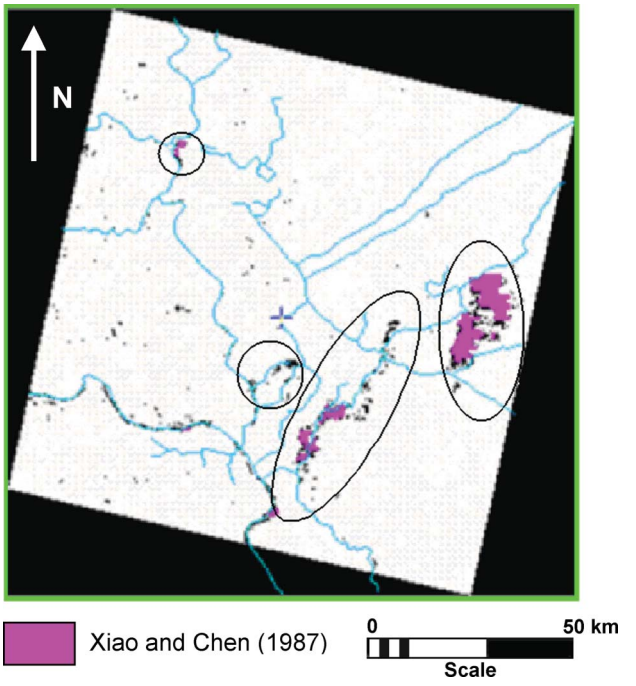

Figure 5. Results obtained by applying the methods proposed by Xiao and Chen (1987) to the AVHRR image of 14 April 2000, 13 GMT over the flooded area corresponding to the green box depicted in figure 2. Rivers have been coloured in cyan. Pink pixels indicate water covered (i.e possibly flooded) locations ($S_0 = -11.5$ %). In the background an adapted version of figure 4 where the dark areas, within the circles, representing the zones mainly affected by floods.

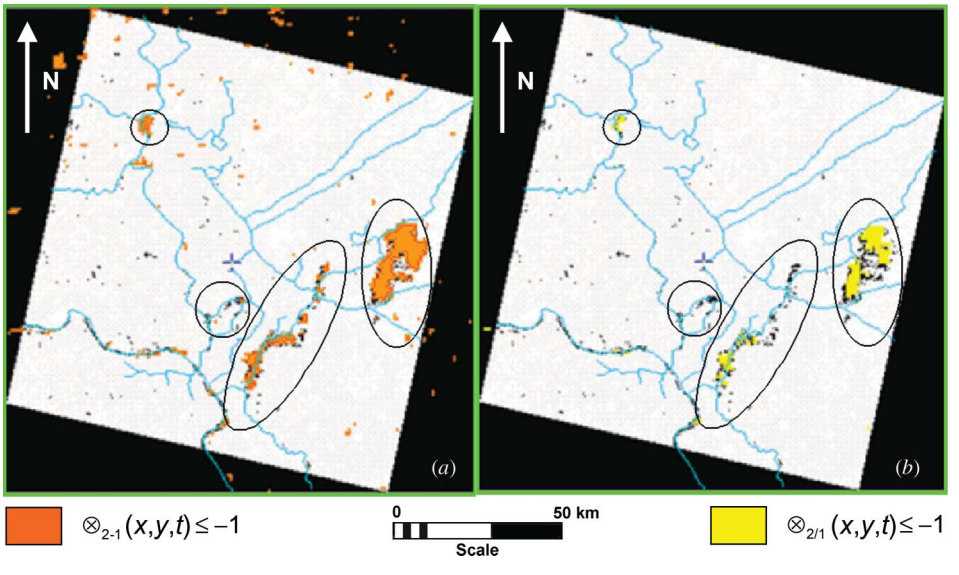

Figure 6. As figure 5, results obtained applying: (*a*) $\otimes_{2\_1}(x,y,t)$ index (orange pixels) and (*b*) $\otimes_{2/1}(x,y,t)$ index (yellow pixels) are shown.

the top of figure 7, results of the application of the methods of Xiao and Chen (1987), Sheng and Xiao (1998) and Verdin (1996) to the area within the red box in figure 2, for the AVHRR images collected on 9 April 2000 at 14:00 GMT, are shown. All these algorithms erroneously identify areas as flooded, which were actually not affected by floods. In this case, snow on the top of mountains (the Dinaric Alps), clouds (which present a spectral response in the AVHRR channels 1 and 2 quite similar to water (Dozier 1989) and cloud shadows played a major role in producing the identification errors. On the bottom of the figure, results applying both RAT indexes are shown: not one pixel is identified as flooded, no false detections are produced. Similar results (figure 8) are obtained for the areas within the blue box for the AVHRR image of 21 April 2000 at 13:00 GMT (note that the results of the Sheng and Xiao (1998) method are not shown for 21 April because, in this case, it was not possible to univocally identify the S_0 threshold for the R_2 / R_1 AVHRR product). Again, the differential nature of our approach allows us to overcome site effects: this result is not unexpected, confirming the intrinsic robustness of the ALICE indexes.

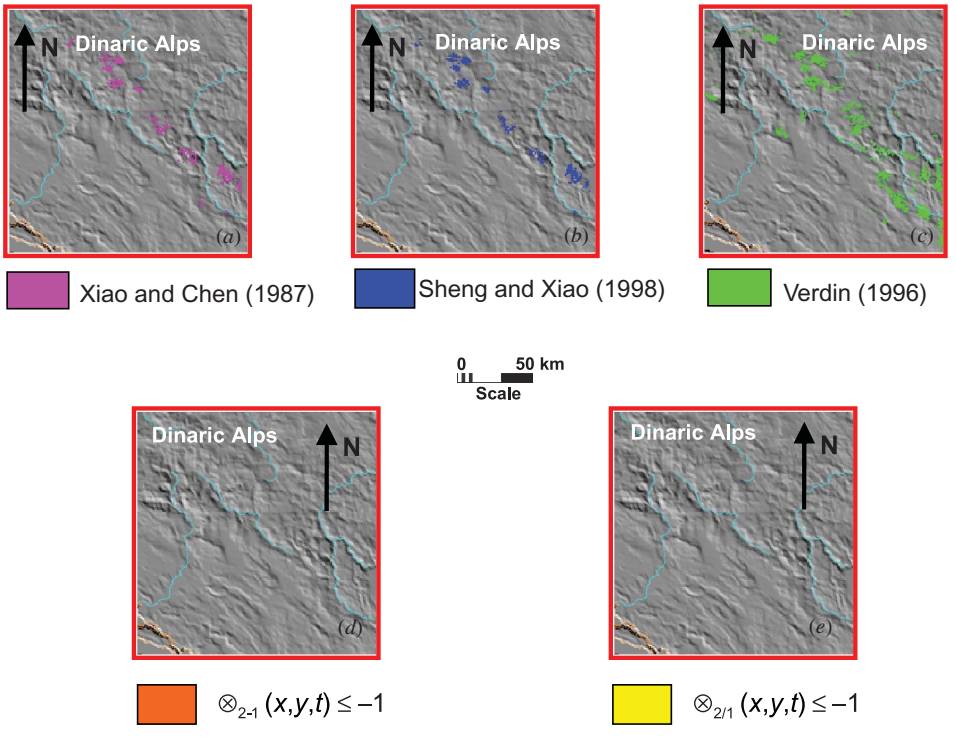

Figure 7. (Top) Results obtained by applying different flooded area mapping methods to the AVHRR image collected on: 9 April 2000, at 14:00 GMT over areas which are not flooded (corresponding to the red boxes depicted in figure 2). Rivers have been coloured in cyan. In particular, results obtained using the method proposed by Xiao and Chen (1987) have been depicted in pink (*a*, $S_0 = 0\%$), those using Sheng and Xiao (1998) in blue (*b*, $S_0 = 1$), while the results found using the method by Verdin 1996 (*c*, $S_0 = 268$ K) have been coloured in green. In background the DEM, courtesy of the U.S. Geological Survey. (Bottom) Results obtained applying the proposed approach are shown. Those achieved using $\otimes_{2\_1}(x,y,t)$ index are plotted in orange (*d*), while pixels identified by $\otimes_{2/1}(x,y,t)$ index have been coloured in yellow (*e*).

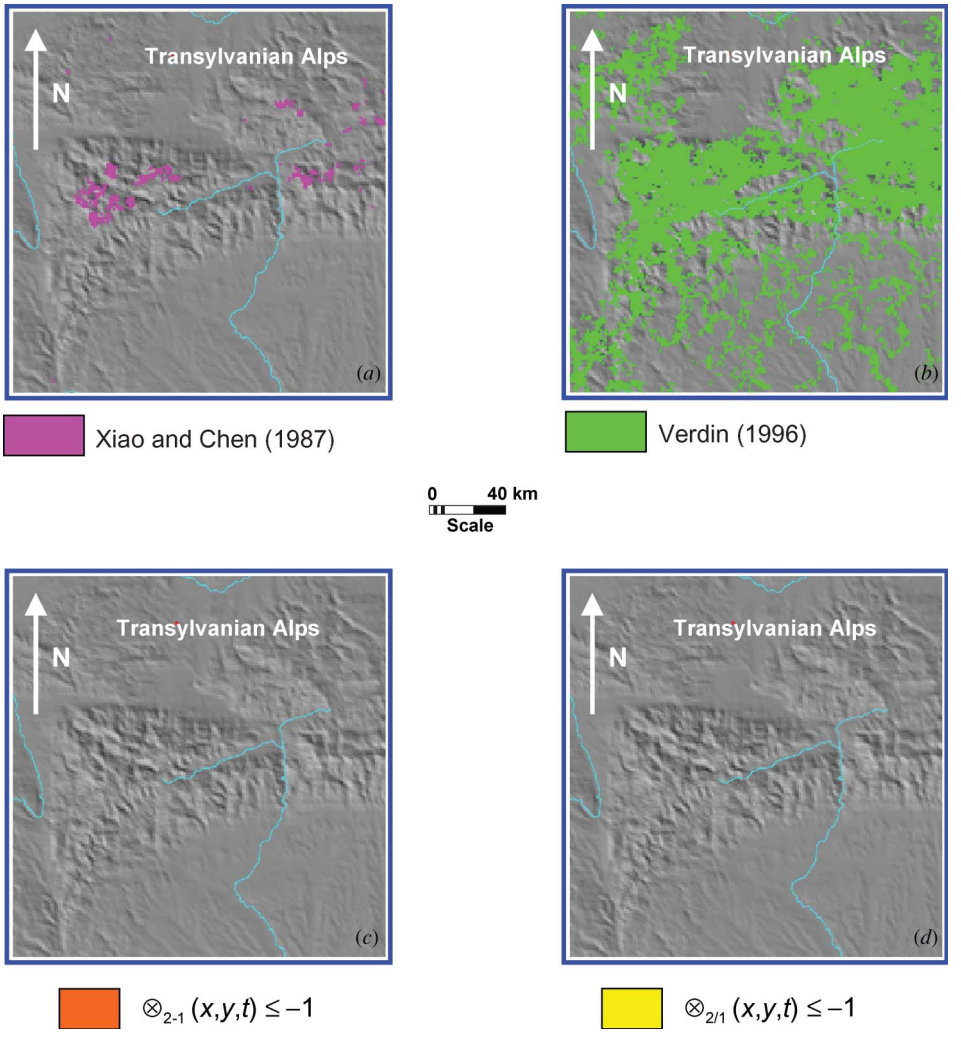

Figure 8. As figure 7 for the AVHRR image acquired on 21 April 2000 at 13:00 GMT, for areas that are not flooded corresponding to the blue boxes depicted in figure 2. In particular, results obtained using the method proposed by: Xiao and Chen (1987) have been depicted in pink (*a*), ($S_0 = -0.5\%$), those using the method by Verdin 1996 (*b*) ($S_0 = 289$ K) have been coloured in green, those achieved using the $\otimes_{2\_1}(x,y,t)$ index are plotted in orange (*c*), while pixels identified by $\otimes_{2/1}(x,y,t)$ index have been coloured in yellow (*d*).

Results of the application of the Xiao and Chen (1987) and Sheng and Xiao (1998) techniques to the AVHRR image collected (around 13:00 GMT) on 9 April 2000 are shown in figure 9. In particular, figures 9(*b*) and 9(*c*) show the detail of the results obtained by such techniques in a flooded area around Kiskoere Lake (figure 9(*a*)). Both techniques are able to correctly identify Kiskoere Lake (within circle B), as well as some flooded areas along the Tisza River (circles A1 and A2). Again, the test highlights the capability of both techniques in identifying water bodies. The presence of flooded areas around Kiskoere Lake is, instead, less evident and, as mentioned previously, further processing steps are required in order to discriminate them from the normal behaviour of the lake water. Using a differential approach, such as the one

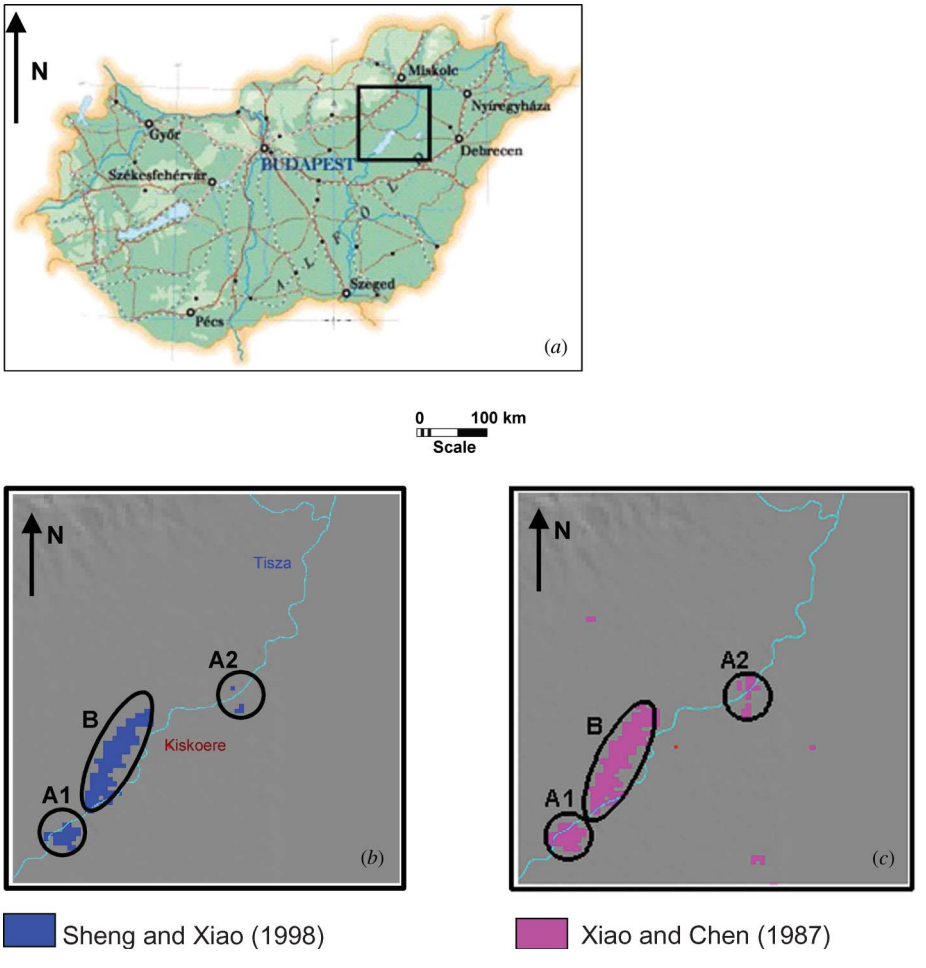

Figure 9. (*a*) Localization of Kiskoere lake. Results obtained by: (*b*) Sheng and Xiao (1998) (in blue), (*c*) Xiao and Chen (1987) (in pink) techniques are shown, respectively, for the areas within the black rectangle in figure 2 and relating to the image of 9 April 2000 at 14 GMT. Rivers have been coloured in cyan. In the background, the DEM courtesy of the U.S. Geological Survey.

proposed in this paper, could help in overtaking such limitations. In figure 10, results obtained by the RAT on the AVHRR image already analysed by the Xiao and Chen (1987) and Sheng and Xiao (1998) techniques (figures 9(*b*) and (*c*)) are shown. The comparison with figures 9(*b*) and 9(*c*) shows that both the $\otimes_{2/1}$ and $\otimes_{2-1}$ ALICE indexes allow us immediately to identify the inundated edges of Kiskoere Lake, discriminating them from the normal behaviour of this water body. This is obviously due to the intrinsic differential nature of the indexes described by expressions (2) and (3) that, in contrast to algorithms devoted to discriminate water from soil, are conceived to identify only variations in water-body presence and extension.

A further comparison of performances achievable by the $\otimes_{2/1}$ and $\otimes_{2-1}$ indexes is offered in figure 11, which permits us to better understand their possible complementarities in an operational detecting-and-mapping scheme.

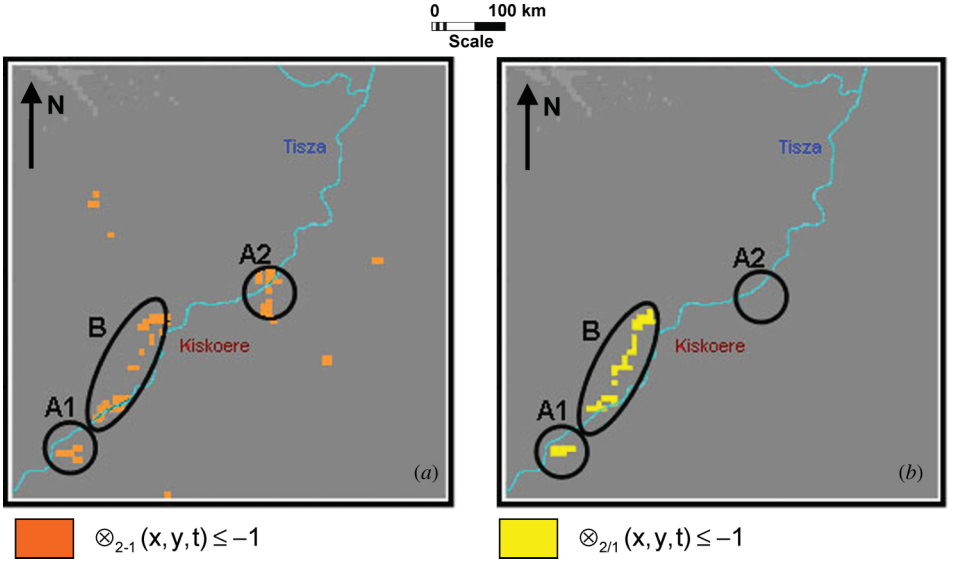

Figure 10. As in figure 9: results obtained with both RAT approaches (pixels colored in orange (*a*) and yellow (*b*), respectively) are shown. The comparison with figures 9(*b*) and 9(*c*), shows as the differential nature of RAT allows us to immediately identify the inundated edges of the Kiskoere lake, discriminating them from the normal behavior of the lake.

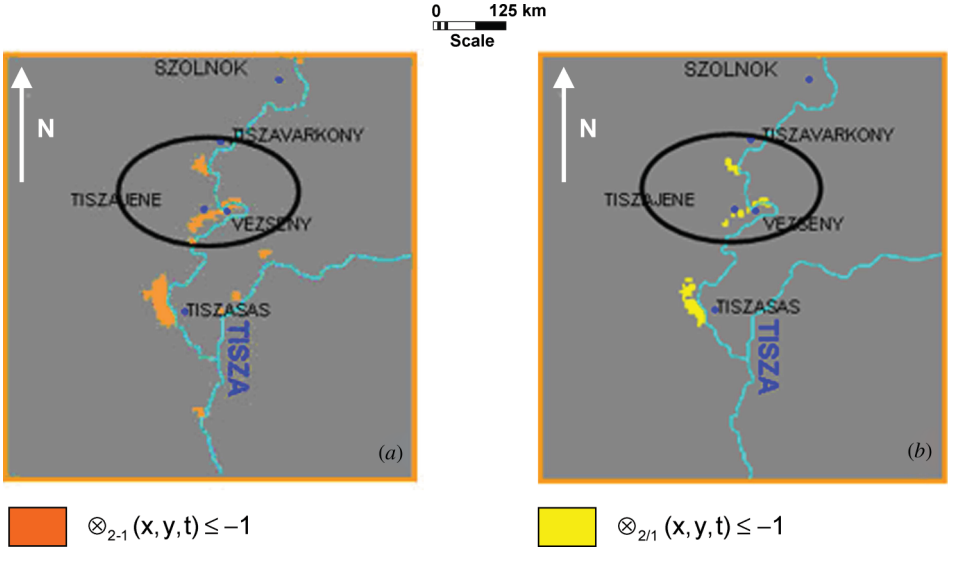

Figure 11. Results obtained applying: (*a*) the $\otimes_{2-1}(x,y,t)$ index (orange pixels) and (*b*) the $\otimes_{2/1}(x,y,t)$ index (yellow pixels) to the AVHRR image of 23 April 2000, 15 GMT (the portions within the orange box of figure 2) are shown. Rivers have been coloured in cyan. For the same area a bulletin describing the flood damages was issued by France Press Agency (2000) on 18 April 2000.

In this figure, in fact, both indexes have been applied to map the state of soils (in the area within the orange box in figure 2), on 23 April, a few days after the peak of the considered flooding event. The processed image refers to the first cloud-free AVHRR image over the considered area after the Bulletin was issued (on 18 April 2000) by France Press Agency (2000), describing the effects of floods affecting the villages of Tiszajenae, Tiszavarkony and Vezseny between Szolnok and Tiszasas. All pixels identified as flooded by the $\otimes_{2/1}$ and $\otimes_{2-1}$ indexes actually correspond to ground reports. Again, the results shown in figure 11 seem to indicate that the $\otimes_{2/1}$ index is more selective in identifying flooded areas than the $\otimes_{2-1}$ index.

Comparing results achieved by using the $\otimes_{2/1}$ and $\otimes_{2-1}$ indexes in figures 6, 10 and 11, it is possible to note that both indexes give quite similar results, with an indication of the major robustness of the $\otimes_{2/1}$ index (against possible false alarms) compared with the major sensitivity of the $\otimes_{2-1}$ index, which seems to indicate more pixels as flooded, even far from the flooded areas identified by using the $\otimes_{2/1}$ index. However, most of these pixels are located very close to the major Tisza River tributaries and to other permanent water bodies so that, in the absence of detailed ground reports, the hypothesis that they are actually flood-affected (more than the result of some spurious effects) seems more likely.

A suitable combination of both the indexes could become a useful tool for flood monitoring. A robust (i.e. low rate of false alarm) identification of flooded areas could be achieved by the $\otimes_{2/1}$ index, while the combination with the $\otimes_{2-1}$ index should help for a wider and more detailed delimitation of the flooded areas.

Finally, as far as a timely and reliable detection of the flooded area is concerned, it is possible to imagine a combined use of both indexes as follows:

- to use the $\otimes_{2/1}$-based products in order to identify flooded areas, with more certainty;
- to use the $\otimes_{2-1}$-based products in order to obtain a more detailed description of affected areas around the pixels previously identified as flooded, with more certainty, and indications of other possibly flooded areas to be submitted to further or independent observations.

6. Conclusions

Satellite observations are a fundamental part of the hydro-meteorological risk management cycle. Different satellite data, in terms of spectral, spatial and temporal features, are required in each single phase. There are, obviously, some critical situations (crisis phase) where timely information is the key request. Meteorological satellites, despite their relatively low spatial resolution (1 to 3 km), offer the highest frequency of passages (from hours to a few minutes) that could effectively help people who have to take a decision quickly about the best strategy in order to minimize the effects of floods.

In this paper, a new AVHRR technique for mapping flooded areas is presented. The proposed approach has been applied to analyse the flooding event that hit the Carpathian Basin during April 2000. Two indexes have been proposed: one based on the difference between the signals measured in AVHRR channels 2 and 1 and the other on the ratio between the same channels.

Preliminary results seem to confirm that this technique is able to reduce the main limitations of the traditional AVHRR methods (Xiao and Chen 1987, Verdin 1996, Sheng and Xiao 1998). The proposed approach, in fact, works automatically without

the need for an operator, and has demonstrated the ability to drastically reduce false identifications arising from site effects, as well as those due to cloud shadows or to the presence of snow. Moreover, the results also show an improvement in the capability to discriminate permanent water bodies from actually flooded areas, with a good sensitivity in the identification of flood-affected soils.

The analysis of the results seems to point out that the joint use of both indexes could allow us to obtain a full identification of the area affected by the flood: first a more robust (without false alarm) identification using the $\otimes_{2/1}$ index of the flooded zones, and second, a wider and more detailed delimitation of all the areas involved in the event using the $\otimes_{2-1}$ index. Such a product could also be useful in the post-crisis phase, both in the estimation of damage and in the definition of new hazard maps.

Finally, an important advantage of this technique is its complete exportability to different geographic areas and satellite packages. In fact, it is based only on satellite data at hand and does not require ancillary data to be implemented. It will then permit us to immediately exploit improved performances offered by the new generation of satellite sensors. In particular, the Spinning Enhanced Visible and Infrared Imager (SEVIRI) aboard the Meteosat Second Generation (MSG) has two channels (channels 1 and 2, respectively) similar to the first two AVHRR channels, with a poor spatial resolution (3 km at nadir), but with a better temporal resolution (15 minutes) that could give effective real-time flood monitoring. In addition, the visible and near infrared channels of the Moderate Resolution Imaging Spectroradiometer (MODIS), flying on the Aqua and Terra mission, could be used to obtain similar information with higher spatial resolution (from 250 to 500 m). Results obtained using these data will be the object of new specific papers. Furthermore, future prospects are also to extend the use of this new technique to thermal infrared channels to obtain continuous monitoring, both during the night and day.

References

Ali, A., 1989, Study of river flood hydrology in Bangladesh with AVHRR data. *International Journal of Remote Sensing*, **10**, pp. 1873–1892.

Barton, I.J. and Bathols, J., 1989, Monitoring floods with AVHRR. *Remote Sensing of Environment*, **30**, pp. 89–94.

Brakenridge, G.R., Anderson, E. and Caquard, S., 2003, *Flood Archives*, (Hanover, USA: Dartmouth Flood Observatory). Available online at: http://www.dartmouth.edu/%7Efloods/Archives/2000sum.xls.

Cao, S., Dong, W. and Xiao, Q., 1987, Applying meteorological satellite imagery to monitor Laohe River flood. *Remote Sensing Information*, **3**, pp. 12–16.

Committee on Earth Observation Satellites (CEOS), 2001, Disaster management support project Earth observation satellites for flood management – flood hazard team report 2001. Available online at: http://www.ceos.org/pages/DMSG/2001Ceos/Reports/flood.html.

Committee on Earth Observation Satellites (CEOS), 2003, The use of Earth observing satellites for hazard support: assessments and scenarios – final report of the CEOS Disaster Management Support Group (DMSG). Available online at: http://www.ceos.org/pages/DMSG/pdf/CEOSDMSG.pdf.

Corrado, R., Caputo, R., Filizzola, C., Pergola, N., Pietrapertosa, C. and Tramutoli, V., 2005, Seismically active areas monitoring by robust TIR satellite techniques: a sensitivity analysis on low magnitude earthquakes occurred in Greece and Turkey since 1995. *Natural Hazards and Earth System Sciences*, **5**, pp. 101–108.

Cuomo, V., Lasaponara, R. and Tramutoli, V., 2001, Evaluation of a new satellite-based method for forest fire detection. *International Journal of Remote Sensing*, **22**, pp. 1799–1826.

Cuomo, V., Filizzola, C., Pergola, N., Pietrapertosa, C. and Tramutoli, V., 2004, A self-sufficient approach for GERB cloudy radiance detection. *Atmospheric Research*, **72**, pp. 39–56.

Dozier, J., 1989, Spectral signature of alpine snow cover from the Landsat Thematic Mapper. *Remote Sensing of Environment*, **28**, pp. 9–22.

Di Bello, G., Filizzola, C., Lacava, T., Marchese, F., Pergola, N., Pietrapertosa, C., Piscitelli, S., Scaffidi, I. and Tramutoli, V., 2004, Robust satellite techniques for volcanic and seismic hazards monitoring. *Annals of Geophysics*, **47**, pp. 49–64.

Domenikiotis, C., Loukas, A. and Dalezios, N. R., 2003, The use of NOAA/AVHRR satellite data for monitoring and assessment of forest fires and floods. *Natural Hazards and Earth System Sciences*, **3**, pp. 115–128.

Filizzola, C., Pergola, N., Pietrapertosa, C. and Tramutoli, V., 2004, Robust satellite techniques for seismically active areas monitoring: a sensitivity analysis on September 7th 1999 Athens's earthquake. *Physics and Chemistry of the Earth*, **29**, pp. 517–527.

France Press Agency, 2000, Hungary: floods – April 2000. Available online at: http://reliefweb.int/rw/dbc.nsf/doc104?OpenForm&rc=4&cc=hun.

Gupta, R.P, 1991, *Remote Sensing Geology* (Berlin, Germany: Springer-Verlag).

Hasegawa, I., Mitomi, Y., Nakayama, Y. and Takeuchi, S., 1998, Land cover analysis using multi seasonal NOAA AVHRR mosaicked images or hydrological applications. *Advances in Space Research*, **22**, pp. 677–680.

Islam, M. and Kimiteru, S., 2000, Flood hazard assessment in Bangladesh using NOAA AVHRR data with GIS. *Hydrological Processes*, **14**, pp. 605–620.

Jain, S.K., Singh, R.D., Jain, M.K. and Lohani, A.K., 2005, Delineation of flood-prone areas using remote sensing techniques. *Water Resources Management*, **19**, pp. 333–347.

Jain, S.K, Saraf, A.K., Goswami, A. and Ahmad, T., 2006, Flood inundation mapping using NOAA AVHRR data. *Water Resource Management*, **20**, pp. 949–959.

Lacava, T., Greco, M., Di Leo, E.V., Martino, G, Pergola, N., Sannazzaro, F. and Tramutoli, V., 2005a, Monitoring soil wetness variations by means of satellite passive microwave observations: the HYDROPTIMET study cases. *Natural Hazards and Earth System Sciences*, **5**, pp. 583–592.

Lacava, T., Greco, M., Di Leo, E.V., Martino, G., Pergola, N., Romano, F., Sannazzaro, F. and Tramutoli, V., 2005b, Assessing the potential of SWVI (Soil Variation Index) for hydrological risk monitoring by satellite microwave observations. *Advances in Geosciences*, **2**, pp. 221–227.

Lacava, T., Cuomo, V., Di Leo, E.V., Pergola, N., Romano, F. and Tramutoli, V., 2005c, Improving soil wetness variations monitoring from passive microwave satellite data: the case of April 2000 Hungary flood. *Remote Sensing of Environment*, **96**, pp. 135–148.

Lacava, T., Di Leo, E.V., Pergola, N. and Tramutoli, V., 2006, Space–time soil wetness monitoring by a multi-temporal microwave satellite records analysis. *Physics and Chemistry of the Earth*, **31**, pp. 1274–1283.

Lin, C., 1989, Applying meteorological satellite information to monitor water-logging in Heilongjiang Province. *Remote Sensing Information*, **3**, pp. 24–28.

Liu, W.T. and Ayres, F.M., 2005, Upper Paraguay River inundation prediction using rainfall and NDVI. *International Journal of Remote Sensing*, **26**, pp. 4455–4470.

McFeeters, S.K.,1996, The use of normalised difference water index (NDVI) in the delineation of open water features. *International Journal of Remote Sensing*, **17**, pp. 1425–1432.

McGinnis, D.F. and Rango, A., 1975, Earth resources satellite system for flood monitoring. *Geophysical Research Letters*, **2**, pp. 132–135.

Pergola, N. and Tramutoli, V., 2000, SANA: sub-pixel automatic navigation of AVHRR imagery. *International Journal of Remote Sensing*, **21**, pp. 2519–2524.

Pergola, N. and Tramutoli, V., 2003, Two years of operational use of subpixel automatic navigation of AVHRR scheme: accuracy assessment and validation. *Remote Sensing of Environment*, **85**, pp. 190–203.

Pergola, N., Pietrapertosa, C., Lacava, T. and Tramutoli, V., 2001, Robust satellite techniques for monitoring volcanic eruptions. *Annals of Geophysics*, **44**, pp. 167–177.

Pergola, N., Tramutoli, V., Scaffidi, I., Lacava, T. and Marchese, F., 2004, Improving volcanic ash clouds detection by a robust satellite technique. *Remote Sensing of Environment*, **90**, pp. 1–22.

Pietrapertosa, C., Pergola, N., Lanorte, V. and Tramutoli, V., 2001, Self adaptive algorithms for change detection: OCA (the One-channel Cloud-detection Approach) an adjustable method for cloudy and clear radiances detection. In *Technical Proceedings of 11th International (A)TOVS Study Conference* (*ITSC-XI*), J.F. Le Marshall and J.D. Jasper (Eds), 20–26 September 2000, Budapest, Hungary (Melbourne, Australia: Bureau of Meteorology Research Centre), pp. 281–291.

Pultz, T.J. and Crevier, Y., 1996, Early demonstration of RADARSAT for applications in hydrology. In *3rd International Workshop on Applications of Remote Sensing in Hydrology*, 16–18 October 1996, Greenbelt, MD, pp. 271–282.

Pultz, T.J., Leconte, R., St Laurent, L. and Peters, L., 1991, Flood mapping with airborne SAR imagery: case of the 1987 St. John River flood. *Canadian Water Resources Journal*, **16**, pp. 173–189.

Pultz, T.J., Crevier, Y., Brown, R.J. and Boisvert, J., 1997, Monitoring of local environmental conditions with SIR-C/X-SAR. *Remote Sensing of the Environment*, **59**, pp. 248–255.

Sandholt, I., Nyborg, L., Fog, B., Lô, M., Bocoum, O. and Rasmussen, K., 2003, Remote sensing techniques for flood monitoring in the Senegal River Valley. *Geografisk Tidsskrift Danish Journal of Geography*, **103**, pp. 71–81.

Saper, R., Pultz, T.J., Crevier, Y., Bowring, R. and Mclauren, I., 1986, Demonstration of RADARSAT potential for flood monitoring – the 1996 Manitoba spring floods. In *3rd International Workshop on Applications of Remote Sensing in Hydrology*, 16–18 October, Greenbelt, MD, pp. 313–322.

Sheng, Y. and Xiao, Q., 1998, Challenging the cloud-contamination problem in flood monitoring with NOAA/AVHRR imagery. *Photogrammetric Engineering and Remote Sensing*, **64**, pp. 191–198.

Sheng, Y. and Gong, P., 2001, Quantitative dynamic flood monitoring with NOAA AVHRR. *International Journal of Remote Sensing*, **22**, pp. 1709–1724.

Tramutoli, V., 1998, Robust AVHRR Techniques (RAT) for Environmental Monitoring: theory and applications. In *Earth Surface Remote Sensing II*, G. Cecchi and E. Zilioli (Eds), vol. 3496 (Bellingham, WA: SPIE), pp. 101–113.

Tramutoli, V., 2005, Robust satellite techniques (RST) for natural and environmental hazards monitoring and mitigation: ten years of successful applications. In *9th International Symposium on Physical Measurements and Signatures in Remote Sensing*, S. Liang, J. Liu, X.N Li, R. Liu and M. Schaepman (Eds), vol. XXXVI (7/W20) (Beijing, China: ISPRS), pp. 792–795.

Tramutoli, V., Di Bello, G., Pergola, N. and Piscitelli, S., 2001, Robust satellite techniques for remote sensing of seismically active areas. *Annals of Geophysics*, **44**, pp. 295–312.

Tramutoli, V., Cuomo, V., Filizzola, C., Pergola, N. and Pietrapertosa, C., 2005, Assessing the potential of thermal infrared satellite surveys for monitoring seismically active areas. The case of Kocaeli (İzmit) earthquake, August 17th, 1999. *Remote Sensing of Environment*, **96**, pp. 409–426.

Verdin, J.P., 1996, Remote sensing of ephemeral water bodies in western Niger 1996. *International Journal of Remote Sensing*, **17**, pp. 733–748.

Wang, Q., Watanabe, M., Hayashi, S. and Murakami, S., 2003, Using NOAA AVHRR data to assess flood damage in China. *Environmental Monitoring and Assessment*, **82**, pp. 119–148.

Winsnet, D.R., McGinnis, D.F. and Pritchard, J.A., 1974, Mapping of the 1973 Mississippi River floods by NOAA-2 satellite. *Water Resources Bulletin*, **10**, pp. 1040–1049.

Xiao, Q. and Chen, W, 1987, Songhua River flood monitoring with meteorological satellite imagery. *Remote Sensing Information*, **4**, pp. 37–41.